J|A|C|S
ARTICLES
Published on Web 09/29/2006

Controlling Gold Atom Penetration through Alkanethiolate Self-Assembled Monolayers on Au{111} by Adjusting Terminal Group Intermolecular Interactions

Zihua Zhu, Thomas A. Daniel, Masato Maitani, Orlando M. Cabarcos, David L. Allara,* and Nicholas Winograd*

Contribution from the Department of Chemistry, The Pennsylvania State University, University Park, Pennsylvania 16802

Received January 13, 2006; E-mail: nxw@psu.edu; dla3@psu.edu

Abstract: The penetration behavior of thermally evaporated Au on $S(CH_2)_{15}CH_3$, $S(CH_2)_{15}CO_2CH_3$, $S(CH_2)_{15}CO_2H$, K-modified $S(CH_2)_{15}CO_2CH_3$, and K-modified $S(CH_2)_{15}CO_2H$ self-assembled monolayers (SAM) on Au substrates is investigated. Gold is a particularly interesting metal since vapor-deposited Au atoms are known to pass through alkanethiolate SAMs on Au{111} substrates at room temperature. Here we show that it is possible to control Au penetration by adjusting the interactions between terminal groups. It is found that Au atoms evenly penetrate into the CH_3 and CO_2CH_3 films, forming smooth buried layers below the organic thin films. For the CO_2H film, although Au atoms can still penetrate through it, filaments and mushroomlike clusters form due to H-bonding between film molecules. In the case of the K-modified CO_2CH_3 or CO_2H films, however, most Au atoms form islands at the vacuum interface. These results suggest that van der Waals forces and H-bonds are not strong enough to block Au from going through but that ionic interactions are able to block Au penetration. The measurements were performed primarily using time-of-flight secondary ion mass spectrometry (ToF−SIMS) and atomic force microscopy (AFM). The combination of these highly complementary probes provides a very useful strategy for the study of metal atom behavior on SAMs.

Introduction

Vapor deposition of Au onto organothiolate self-assembled monolayers (SAMs) on Au{111} with various terminal groups is a common approach to preparing a Au/SAM/Au substrate sandwich structure.[1] Gold, however, is known to pass through most SAMs very easily at room temperature.[2−6] In particular, scanning tunneling microscope measurements[4−6] have shown that Au penetration is especially severe for simple CH_3-terminated SAMs. Theoretical calculations show that, for these types of SAMs where the molecular chains interact solely by weak van der Waals forces, room temperature thermal energy can cause small fluctuations in the lateral positions of the film molecules on the Au substrate.[7,8] This movement results in temporary vacancies, and the sizes of such vacancies are large enough for metal atoms to leak from the vacuum interface to the Au/S interface.[9]

One possible means to alter metal penetration is to enhance the interactions between vapor-deposited Au atoms and surface organic functional groups. For example, Au is found to form clusters at the vacuum interface when deposited on SH-terminated SAMs.[4,10,11] Decreasing the substrate temperature is an alternative way to reduce the mobility of the SAM molecules. For example, Reed and co-workers cooled the SAM samples to liquid-N_2 temperature to avoid Au atoms punching through the films.[1] In this paper, we examine the possibility of controlling Au penetration by varying the chemical and ionic interactions between the terminal portions of the molecules at the SAM−ambient interface while leaving the interior intermolecular interactions and the substrate interfaces unchanged.

To test this idea, Au was deposited onto SAMs prepared on Au{111} substrates by adsorption of $S(CH_2)_{15}CH_3$, $S(CH_2)_{15}CO_2CH_3$, and $S(CH_2)_{15}CO_2H$ and onto the K-modified $S(CH_2)_{15}CO_2CH_3$ and K-modified $S(CH_2)_{15}CO_2H$ SAMs. This combination allows the effects of van der Waals forces, H-bonding, and ionic interactions on Au penetration to be determined in detail. For CH_3- and CO_2CH_3-terminated films, the interaction between molecules is largely a van der Waals interaction, with perhaps minor contributions from weak electric dipole forces for the ester group. For CO_2H-terminated films, H-bonding

(1) For an example in molecular electronics, see the following: Chen, J.; Reed, M. A.; Rawlett, A. M.; Tour, J. M. *Science* **1999**, *286*, 1550−1552.
(2) Jung, D. R.; Czanderna, A. W. *Crit. Rev. Solid State* **1994**, *19*, 1−54.
(3) Herdt, G. C.; King, D. E.; Czanderna, A. W. *Z. Phys. Chem. (Muenchen)* **1997**, *202*, 163−196.
(4) Ohgi, T.; Sheng, H. Y.; Nejoh, H. *Appl. Surf. Sci.* **1998**, *132*, 919−924.
(5) Ohgi, T.; Sheng, H. Y.; Dong, Z. C.; Nejoh, H. *Surf. Sci.* **1999**, *442*, 277−282.
(6) Wang, B.; Xiao, X. D.; Sheng, P. *J. Vac. Sci. Technol., B* **2000**, *18*, 2351−2358.
(7) Bhatia, R.; Garrison, B. J. *Langmuir* **1997**, *13*, 765−769.
(8) Bhatia, R.; Garrison, B. J. *Langmuir* **1997**, *13*, 4038−4043.
(9) Hooper, A.; Fisher, G. L.; Konstadinidis, K.; Jung, D.; Nguyen, H.; Opila, R.; Collins, R. W.; Winograd, N.; Allara, D. L. *J. Am. Chem. Soc.* **1999**, *121*, 8052−8064.
(10) Ohgi, T.; Sheng, H. Y.; Dong, Z. C.; Nejoh, H.; Fujita, D. *Appl. Phys. Lett.* **2001**, *79*, 2453−2455.
(11) de Boer, B.; Frank, M. M.; Chabal, Y. J.; Jiang, W. R.; Garfunkel, E.; Bao, Z. *Langmuir* **2004**, *20*, 1539−1542.

10.1021/ja060084x CCC: $33.50

between CO_2H groups is known to occur[12,13] and these interactions provide a cross-linked network across the surface whose energies exceed thermal energy at room temperature by perhaps 1 order of magnitude. Our previous work shows that CO_2K moieties form after K is vapor deposited on CO_2CH_3- or CO_2H-terminated SAM and the $-(CH_2)_n-$ chains do not react with K atoms.[14,15] Thus, the interactions between the molecules of K-modified CO_2CH_3 or CO_2H films are mainly ionic interactions arising from the $-CO_2^-$ and K^+ ion layer. The net interactions could be repulsive or attractive depending on the exact positioning of the ions.

Many surface characterization techniques have been applied to investigate metal reactivity with SAMs, such as time-of-flight secondary ion mass spectrometry (ToF−SIMS),[9,16−23] X-ray photoelectron spectroscopy (XPS),[9,11,12,16,17,20,22,24−33] ion scattering spectroscopy (ISS),[25,33−35] infrared reflection spectroscopy (IRS),[9,11,12,17,20,21,36] scanning tunneling microscopy (STM),[4−6,10,37] atomic force microscopy (AFM),[12,17,38−43] and near-edge X-ray absorption fine structure spectroscopy (NEXAFS).[44] Here, we focus on ToF−SIMS and AFM due to their complementarity in characterization of the chemistry and physical structure of the metal/SAM interfaces.

In previous work, we utilized ToF−SIMS to examine the behavior of Al, Ag, Cu, K, Ti, and other metals on a number of alkanethiol SAMs.[9,14−23] The special advantage of these studies is that the molecular specificity associated with the mass spectra can be utilized to acquire detailed structural information especially when comparing our data with those from other techniques. For example, $AlOCH_3^+$ ions are an indicator that deposited Al atoms on an OCH_3-terminated film remain on top, and $AlSH_2^+$ ions are an indicator that Al penetrates through the film to the Au/S interface. Other types of cluster ions are also indicative of specific types of reaction chemistry. TiC^+ ions are found after Ti is deposited on an OCH_3 SAM, indicating that Ti atoms damage the organic functional groups. When K is deposited on $S(CH_2)_{15}CO_2CH_3$ and $S(CH_2)_{15}CO_2H$ films, the disappearance of molecular peaks and the increase of the $S(CH_2)_{15}CO_2K^-$ peak indicate that CO_2CH_3 and CO_2H groups react with K atoms to form CO_2K groups. Additionally, when K is evaporated on CH_3-, CO_2CH_3-, and CO_2H-terminated films, the K^+ signal from the CH_3 film is weaker than that seen on the other two films, suggesting that the sticking coefficient of K atoms on the CH_3 surface is low. Hence, there are a range of characteristic mass spectral peaks that provide simple and direct information about chemistry and structure.

Topography information on these types of systems is usually provided with AFM or STM.[12,17,38−43] Moreover, conductance probe AFM (CPAFM) yields local conductivity information, which could reveal the presence of metallic filaments embedded through the SAM. These filaments would cause unpredictable and undesireable electrical effects in molecular electronic device structures. Hence, the merging of ToF−SIMS with AFM provides a powerful combination of techniques for revealing the structure of metal−organic contacts.

In this paper, a series of experiments are performed with ToF−SIMS where Au is evaporated on $S(CH_2)_{15}CH_3$, $S(CH_2)_{15}CO_2CH_3$, $S(CH_2)_{15}CO_2H$, K-modified $S(CH_2)_{15}CO_2CH_3$, and K-modified $S(CH_2)_{15}CO_2H$ SAMs, respectively. No new mass peaks are found in any of the SAMs under study, suggesting that Au does not induce bond-breaking chemical reactions. After carefully analyzing the intensities of characteristic peaks, we find that Au atoms continuously penetrate through the $S(CH_2)_{15}CH_3$ and $S(CH_2)_{15}CO_2CH_3$ films, forming smooth underlayers below the organic thin films. Additionally, Au atoms partially penetrate through the $S(CH_2)_{15}CO_2H$ film and form filaments and mushroomlike clusters, some of which are in electrical contact with the Au substrate. However, Au atoms do not penetrate through K-modified $S(CH_2)_{15}CO_2CH_3$ and $S(CH_2)_{15}CO_2H$ films as readily and form islands at the vacuum interface. To obtain direct topography and local conductivity properties, normal contact AFM and CPAFM were utilized to study the Au behavior on the $S(CH_2)_{15}CO_2H$ and K-modified $S(CH_2)_{15}CO_2H$ films. Our results show that variation of the terminal group interactions can be an effective way to regulate Au penetration for organothiolate/Au{111} SAMs. Further, since

(12) Smith, E. L.; Alves, C. A.; Anderegg, J. W.; Porter, M. D.; Siperko, L. M. *Langmuir* **1992**, *8*, 2707−2714.
(13) Nuzzo, R. G.; Dubois, L. H.; Allara, D. L. *J. Am. Chem. Soc.* **1990**, *112*, 558−569.
(14) Zhu, Z.; Haynie, B. C.; Winograd, N. *Appl. Surf. Sci.* **2004**, *231−2*, 318−322.
(15) Zhu, Z. Ph.D. Thesis, Penn State University, 2006.
(16) Fisher, G. L.; Hooper, A. E.; Opila, R. L.; Allara, D. L.; Winograd, N. *J. Phys. Chem. B* **2000**, *104*, 3267−3273.
(17) Fisher, G. L.; Walker, A. V.; Hooper, A. E.; Tighe, T. B.; Bahnck, K. B.; Skriba, H. T.; Reinard, M. D.; Haynie, B. C.; Opila, R. L.; Winograd, N.; Allara, D. L. *J. Am. Chem. Soc.* **2002**, *124*, 5528−5541.
(18) Haynie, B. C.; Walker, A. V.; Tighe, T. B.; Allara, D. L.; Winograd, N. *Appl. Surf. Sci.* **2003**, *203−204*, 433−436.
(19) Walker, A. V.; Tighe, T. B.; Reinard, M. D.; Haynie, B. C.; Allara, D. L.; Winograd, N. *Chem. Phys. Lett.* **2003**, *369*, 615−620.
(20) Walker, A. V.; Tighe, T. B.; Cabarcos, O. M.; Reinard, M. D.; Haynie, B. C.; Uppili, S.; Winograd, N.; Allara, D. L. *J. Am. Chem. Soc.* **2004**, *126*, 3954−3963.
(21) Walker, A. V.; Tighe, T. B.; Stapleton, J.; Haynie, B. C.; Uppili, S.; Allara, D. L.; Winograd, N. *Appl. Phys. Lett.* **2004**, *84*, 4008−4010.
(22) Walker, A. V.; Tighe, T. B.; Haynie, B. C.; Uppili, S.; Winograd, N.; Allara, D. L. *J. Phys. Chem. B* **2005**, *109*, 11263−11272.
(23) Tighe, T.; Daniel, T.; Zhu, Z.; Upilli, S.; Winograd, N.; Allara, D. L. *J. Phys. Chem. B* **2005**, *109*, 21006−21014.
(24) Czanderna, A. W.; King, D. E.; Spaulding, D. *J. Vac. Sci. Technol., A* **1991**, *9*, 2607−2613.
(25) Tarlov, M. J. *Langmuir* **1992**, *8*, 80−89.
(26) Jung, D. R.; King, D. E.; Czanderna, A. W. *Appl. Surf. Sci.* **1993**, *70-1*, 127−132.
(27) Jung, D. R.; King, D. E.; Czanderna, A. W. *J. Vac. Sci. Technol., A* **1993**, *11*, 2382−2386.
(28) King, D. E.; Czanderna, A. W.; Spaulding, D. *J. Vac. Sci. Technol., A* **1993**, *11*, 180−182.
(29) Jung, D. R.; Czanderna, A. W. *J. Vac. Sci. Technol., A* **1994**, *12*, 2402−2409.
(30) Konstadinidis, K.; Zhang, P.; Opila, R. L.; Allara, D. L. *Surf. Sci.* **1995**, *338*, 300−312.
(31) Herdt, G. C.; Czanderna, A. W. *J. Vac. Sci. Technol., A* **1995**, *13*, 1275−1280.
(32) Razafitrimo, H.; Ettedgui, E.; Guo, L. H.; McLendon, G. L.; Gao, Y. *Appl. Phys. Lett.* **1995**, *67*, 2621−2623.
(33) Dake, L. S.; King, D. E.; Czanderna, A. W. *Solid State Sci.* **2000**, *2*, 781−789.
(34) Herdt, G. C.; Czanderna, A. W. *J. Vac. Sci. Technol., A* **1994**, *12*, 2410−2414.
(35) Herdt, G. C.; Czanderna, A. W. *Surf. Sci.* **1993**, *297*, L109−L112.
(36) Colavita, P. E.; Doescher, M. S.; Molliet, A.; Evans, U.; Reddic, J.; Zhou, J.; Chen, D.; Miney, P. G.; Myrick, M. L. *Langmuir* **2002**, *18*, 8503−8509.
(37) Ohgi, T.; Fujita, D.; Deng, W.; Dong, Z. C.; Nejoh, H. *Surf. Sci.* **2001**, *493*, 453−459.
(38) Dunaway, D. J.; McCarley, R. L. *Langmuir* **1994**, *10*, 3598−3606.
(39) Lin, H.; Ando, H.; Seo, W. S.; Kuwabara, K.; Koumoto, K. *Thin Solid Films* **1996**, *282*, 521−524.
(40) Yang, D. Q.; Sacher, E.; Griswold, E. M.; Smith, G. *Appl. Surf. Sci.* **2001**, *180*, 200−208.
(41) Carlo, S. R.; Perry, C. C.; Torres, J.; Wagner, A. J.; Vecitis, C.; Fairbrother, D. H. *Appl. Surf. Sci.* **2002**, *195*, 93−106.
(42) Hatton, R. A.; Willis, M. R.; Chesters, M. A.; Briggs, D. *J. Mater. Chem.* **2003**, *13*, 722−726.
(43) Lau, C. N.; Stewart, D. R.; Bockrath, M.; Williams, R. S. *Appl. Phys. A* **2005**, *80*, 1373−1378.
(44) Wacker, D.; Weiss, K.; Kazmaier, U.; Woll, C. *Langmuir* **1997**, *13*, 6689−6696.
(45) Dubois, L. H.; Nuzzo, R. G. *Annu. Rev. Phys. Chem.* **1992**, *43*, 437−463.

the fundamental molecular packing and surface densities of the CO_2H and K-modified CO_2H SAMs must be identical because the same SAM is used for both experiments, it is clear that static defects such as pinholes have little effect on the metal atom penetration processes.

Experimental Section

SAM Preparation. The procedure for preparing the $S(CH_2)_{15}CO_2CH_3$, $S(CH_2)_{15}CO_2H$, and $S(CH_2)_{15}CH_3$ SAMs has been described in detail previously.[9,16] Briefly, an ~10 nm Cr adhesion layer was thermally deposited onto cleaned Si(001) wafers followed immediately by ~200 nm of Au. The freshly deposited Au substrates were removed, typically immediately characterized by single wavelength ellipsometry (70° angle of incidence and 632.8 nm light), and then immersed into 1.0 mM ethanol solutions of the alkanethiol molecules for ~1−2 days at room temperature. The samples were removed from the solutions, thoroughly rinsed with ethanol, sonicated further for 20 s to help remove surface contaminants, and finally dried by blowing with pure N_2. In some cases (particularly for AFM), to rigorously remove physisorbed solute molecules the samples were immersed in 0.02 M HCl (concentrated aqueous acid diluted in ethanol) for 2 min and then rinsed with ethanol and blown dry with N_2. The films were characterized with single-wavelength ellipsometry and contact angle measurements with water to ensure that the surfaces were clean and reproducible sample to sample. Infrared spectroscopy measurements also were run on a number of these samples as an additional characterization. In all cases the IR spectra were identical with those in our previous reports.[16] For the ToF−SIMS experiments, the samples were put into the vacuum chamber and first characterized by ToF−SIMS prior to metal deposition. In the case of the AFM experiments, Au/mica samples (Agilent/Molecular Imaging, Tempe, AZ) were flame annealed immediately prior to SAM formation to form large, atomically flat terraces for obtaining high-resolution images and optimum conductance measurements. After removal from the thiol solutions, the samples were rinsed with ethanol, blown dry with N_2, and immediately loaded into the AFM forechamber, and then the surface was imaged prior to metal deposition. For convenience, the above films are referred to as CO_2CH_3, CO_2H, and CH_3 films, respectively.

Definition of Metal Coverages. For all experiments, the amount of metal delivered/unit area to the samples was determined directly from the QCM measurements as mass/unit area (ρ_A). For convenience in discussing the stoichiometry of metal−SAM interactions, a coverage of one deposited metal atom/SAM molecule was defined as an equivalent layer (EL) and calculated from the QCM data using the ρ_A values, the atomic masses, and the molecular packing density of 4.6 molecules·nm^{-2} for a well-formed alkanethiolate/Au(111) SAM.[45] For all the SAM molecules used the terminal groups are sufficiently small that the ideal packing densities can be assumed to be equal.

ToF−SIMS Experiment. Time-of-Flight Secondary Ion Mass Spectrometer. The ToF−SIMS instrument has been described previously.[46] Briefly, the instrument consists of a loadlock, a metal deposition chamber, a preparation chamber, and a primary analysis chamber, each separated by a gate valve. Gallium ions of 15 keV were used as primary ions. The ions were focused onto a 200 nm diameter beam that was rastered over a 300 × 300 μm^2 area during data acquisition. All spectra were acquired using a total ion dose of less than 10^{11} ions/cm^2. The relative standard deviation of peak intensities is within ±15% from both sample-to-sample and scan-to-scan. In all measurements, the base pressure in the analysis chamber is about 5.0×10^{-10} Torr.

Metal Deposition Chamber. Two metal sources were located side-by-side about 50 cm vertically above the SAM samples. The distance between the two sources is about 5 cm, and they are separated by a 1 mm thick stainless steel shutter. One source consists of a tungsten basket filled with a Au slug (Aldrich, 99.99%). The other source is a K dispenser (SAES getters). Metal dose was monitored by a quartz crystal microbalance (QCM; Maxtek TM400 controller, 6 MHz crystal with rough Au surface). For the gold deposition the metal was deposited to the desired coverage at a constant rate of ~0.15 EL·s^{-1}, identical within errors to the AFM deposition rates. For the K depositions, the metal was deposited at a rate of ~0.006 EL·s^{-1}.

Experimental Procedure. In our study, film samples (CO_2CH_3, CO_2H, and CH_3, each about 6 mm×6 mm) were immobilized on a sample block and were placed into vacuum. The SIMS spectra of freshly prepared monolayers were taken as a control, and then the samples were transferred under vacuum to the metal deposition chamber. After Au deposition, the samples were transferred back to the analysis chamber to acquire SIMS spectra. Each transfer time was about 4−6 min. The pressure of the deposition chamber before Au deposition was about 1.1×10^{-9} Torr and was $< 1.0 \times 10^{-7}$ Torr during Au deposition. After SIMS analysis, the samples were redosed with additional Au. This process was repeated several times until the total Au dose reached about 50 ELs.

For the K-modified CO_2CH_3 and CO_2H SAMs, after deposition of 1.2 EL of K the samples were transferred to the analysis chamber, SIMS measurements obtained, and the samples then returned to the metal deposition chamber for Au deposition. Au deposition and subsequent SIMS measurements were performed in the same fashion as described previously. Previous TOF−SIMS experiments show that 1.2 EL of K converts nearly all CO_2H groups into CO_2K groups and 50−60% of CO_2CH_3 groups into CO_2K groups.[14,15] In addition, in-situ infrared reflection spectroscopy confirm these results (see Supporting Information).

AFM Experiment. AFM Instrument. Measurements were performed in an ultrahigh vacuum (UHV) chamber (base pressure 10^{-10} Torr) outfitted with a RHK 350 scan head and an RHK SPM 100 electronics system (RHK technologies, Troy, MI). Since the scans were done under UHV conditions, the useful modes were contact (as opposed to tapping) and conductance probe. The contact mode AFM images were taken with silicon cantilevers (FMR type, spring constant ~2.8 N/m, tip radius ~10 nm; Agilent/Molecular Imaging, Tempe, AZ). The CPAFM images were taken with electrically conducting platinum−iridium (90/10) coated Si cantilevers (EFM type, spring constant ~3.0 N/m, tip radius ~20 nm, Agilent/Molecular Imaging, Tempe, AZ). The $I-V$ responses of the tip−gold substrate junctions of the samples were monitored using standard picoammeter instrumentation. The scan head was calibrated in the z direction using Au single step edges (0.3 nm height). The x and y lateral directions were calibrated using lattice images of dodecanethiolate monolayers on Au(111).[47,48] Samples were imaged in no fewer than 5 different locations for each experiment, and at least 3 sample for each different deposition amount were analyzed.

Metal Deposition. The deposition chamber consisted of the sample holder, mounted on a transfer arm, a QCM crystal, and controller (Sigma Instruments SQM-160, maximum error ±7%). The chamber was isolated from the main analysis chamber by a gate valve and during depositions the pressure remained $< 5 \times 10^{-7}$ Torr. Geometric factor calibrations (tooling factors) for the placement of the QCM crystal relative to the sample and the metal source were done using AFM measured film thicknesses at the sample and QCM crystal locations. Independent measurements showed that all K or Au atoms impinging on the SAM surfaces were completely adsorbed.

Experimental Procedure. The samples were loaded into the deposition chamber and then immediately transferred in vacuo to the main analysis chamber where they were initially imaged in contact mode using a Si tip since the Si tips are both sharper and more durable than the metal-coated conducting tips. Following imaging of the

(46) Braun, R. M.; Blenkinsopp, P.; Mullock, S. J.; Corlett, C.; Willey, K. F.; Vickerman, J. C.; Winograd, N. *Rapid Commun. Mass Spectrom.* **1998**, *12*, 1246.
(47) Delamarche, E.; Michel, B.; Gerber, C.; Anselmetti, D.; Guntherodt, H. J.; Wolf, H.; Ringsdorf, H. *Langmuir* **1994**, *10*, 2869−2871.
(48) Poirier, G. E.; Tarlov, M. J. *Langmuir* **1994**, *10*, 2853−2856.

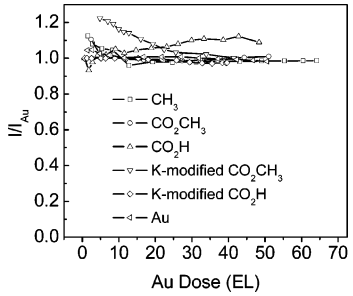

Figure 1. Sticking coefficients of Au atoms on CH_3, CO_2CH_3, CO_2H, and 1.2 EL of K-modified CO_2CH_3 and CO_2H films as a function of Au dose on the bare Au electrode of the reference QCM crystal.

uncoated monolayer, the samples were transferred back to the metal deposition chamber where metal was deposited to the desired coverage at a constant rate of ~0.15 EL·s^{-1}, identical within errors to the ToF−SIMS deposition rates. The metal/SAM sample was then transferred under vacuum back to the main chamber and characterized either by contact mode for topography or by conductance mode (CPAFM) for tip−substrate current imaging. Since tip wear was observed to be significant in CPAFM mode, a tip retract approach mode was used[49] to increase the lifetime of the tip. Once surface contact was established, force−distance measurements were used to verify the tip integrity and damaged tips were discarded.[50] For a given sample, either a bare or K-coated CO_2H SAM, continued deposition and analysis cycles were done with nominally 1, 5, 10, and 20 EL of Au (atoms/SAM molecule) in the same run.

Sticking Coefficient Determination. Measurement of sticking coefficients was carried out to ensure that the metal atom coverages were accurate. A special chamber was constructed with two QCM heads (6 MHz crystals) each equipped with ~200 nm Au electrodes (~10 nm Cr adhesion layer) configured side-by-side, equidistant ~50 cm under the Au source. A hand-controlled shutter was positioned ~2 cm over the QCM heads. The first crystal, with a standard rough Au surface, serves as the reference. The second crystal was prepared by deposition of gold onto a high polish QCM crystal (Cold Springs R&D, Syracuse, NY; rms roughness 0.1−0.2 nm) followed by SAM formation to give a final rms roughness of ~1−2 nm, similar to that of our standard SAM samples on silicon wafers. In an experiment, the reference gold crystal was first covered with fresh gold to ensure that the sticking coefficient would be unity on the surface; then both crystals were simultaneously exposed to the Au vapor and metal thicknesses on both crystals were measured. The sticking coefficient was then determined for the SAM by ratioing the metal thickness on the SAM crystal to that on the bare Au electrode of the reference crystal. The Au deposition rates were controlled to the standard values used for the SIMS and AFM experiments. The results shown in Figure 1 clearly show that the sticking coefficient is the same for all our SAM surfaces within an uncertainty of about 10%.

(49) The scan head has two separate *z* piezos, one for scan off sets and coarse approach *Z* steps and another for scanning the *z* direction only. The tip approached the surface in tip-retract mode. The scan head would take one course *z* step with the *z*-scan piezo fully retracted. After the course *z* step was performed, the *z*-scan piezo is extended with a low gain ensuring that the tip moves at a low speed. If the tip extended into the surface, the approach would then stop. If no normal force change was detected, indicating the presence of the surface, the tip would be fully retracted again and another course *Z* step taken. This is repeated until the substrate surface is found; if faster approach modes are used, the metal tip will be blunted or other wise damaged leading to inconsistent contact areas and current measurements.

(50) The force distance curves are used as a relative measure of the tip radius of curvature. The higher the radius of curvature, the higher the surface area between the tip and the substrate is. For damaged tips the adhesive force was determined to be 5−20 times higher than that of new clean tips (~10 nN). If a high adhesive force was found and was repeatable in different locations of the surface (done to ensure that the tip is not just at a local defect causing higher forces), then the tip was removed from vacuum, discarded, and replaced.

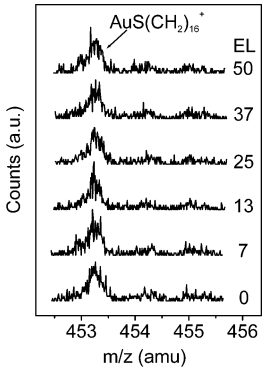

Figure 2. $AuS(CH_2)_{16}^+$ ToF−SIMS spectra obtained from a CH_3 film with increasing amounts of Au deposition.

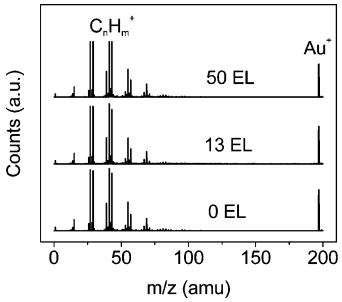

Figure 3. Positive ion ToF−SIMS spectra of a CH_3 film with Au dose for 0, 13, and 50 EL of Au.

Results and Discussion

ToF−SIMS. ToF−SIMS spectra of freshly prepared CH_3, CO_2CH_3, and CO_2H films on Au substrates have been described elsewhere.[9,16,17,51−55] Briefly, characteristic peaks include $C_nH_m^{\pm}$, S^-, SH^-, $SC_nH_m^{\pm}$, $Au_n^{\pm}$, $Au_nS_mH_l^{\pm}$, $AuC_nH_m^{\pm}$, $AuSC_nH_m^{\pm}$, $AuM^{\pm}$, Au_2M^-, and AuM_2^- (M = $S(CH_2)_{15}X$; X = CH_3, CO_2CH_3, and CO_2H). K-modified CO_2CH_3 and CO_2H films have been studied by ToF−SIMS previously,[14,15] and the characteristic peaks are K^+, K_2^+, K_2O^+, $(CH_2)_nCO_2K_2^+$, $Au_nK_m^{\pm}$, $AuC_nH_m^{\pm}$, $AuS(CH_2)_{15}CO_2K^-$, and $(CH_2)_nCO_2^-$.

Au on CH_3 SAM. A partial spectrum of the CH_3 film following varying amounts of Au deposition is shown in Figure 2. The shape and intensity of the $AuS(CH_2)_{16}^+$ peak remains constant with Au deposition. Furthermore, the entire positive ion spectrum (in our experiment m/z = 0−1000) changes only slightly even after 50 EL of Au deposition. This observation can be seen in the positive ion spectra between m/z = 0 and 200 as shown in Figure 3. The negative ion spectra similarly change only slightly during Au deposition, e.g., as shown for $Au_2S(CH_2)_{15}CH_3^-$ in Figure 4. These results show the basic structure of the SAM does not change. Further, since SIMS signals only arise from a few atomic layers in metal films, compared to as many as several nanometers for organic films, the lack of significant changes in the molecular signals clearly indicate that little, if any, Au has accumulated on top of the SAM. A simple calculation shows that ~50 EL of Au atoms

(51) Tarlov, M. J.; Newman, J. G. *Langmuir* **1992**, *8*, 1398−1405.
(52) Hagenhoff, B.; Benninghoven, A.; Spinke, J.; Liley, M.; Knoll, W. *Langmuir* **1993**, *9*, 1622−1624.
(53) Hutt, D. A.; Cooper, E.; Leggett, G. J. *J. Phys. Chem. B* **1998**, *102*, 174−184.
(54) Wolf, K. V.; Cole, D. A.; Bernasek, S. L. *J. Phys. Chem. B* **2002**, *106*, 10382−10387.
(55) Wolf, K. V.; Cole, D. A.; Bernasek, S. L. *Anal. Chem.* **2002**, *74*, 5009−5016.

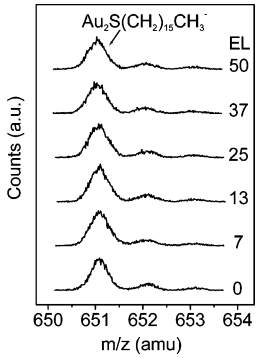

Figure 4. $Au_2S(CH_2)_{15}CH_3^-$ ToF−SIMS spectra obtained from a CH_3 film with increasing amounts of Au deposition.

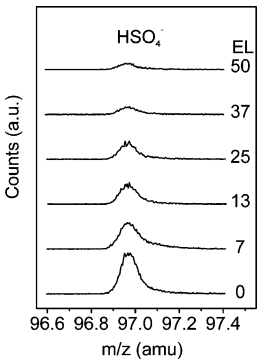

Figure 5. HSO_4^- ToF−SIMS spectra obtained from a CH_3 film with increasing amounts of Au deposition.

can form 17 single (111) terrace layers; thus Au atoms exhaustively penetrate through the CH_3 film, and the film appears to "float" on these deposited atoms. Additionally, no new ion peaks are found during Au deposition, either positive or negative, indicating that no chemical reactions occur during Au evaporation, as expected. All these observations are consistent with previous reports that vapor-deposited Au atoms penetrate through a number of different alkanethiol SAMs on Au substrates to form smooth underlayers between the original Au substrate and the organic thin layer.[2−6,11,21]

SO_3^- and HSO_4^- are weak peaks and are commonly found if the CH_3 sample is prepared in an ambient environment. The appearance of these peaks indicates that a small number of −SH groups are oxidized.[53−55] An interesting observation is that these peaks decrease significantly with Au deposition (Figure 5) whereas most other negative ion peaks decrease only slightly during this process.[56]

Au on CO_2CH_3 SAM. Gold deposition onto a CO_2CH_3 film yields results that are similar to those for the CH_3 film. Both positive and negative ion spectra undergo slight changes during Au deposition. Two characteristic peaks, $HAuS(CH_2)_{15}CO_2CH_3^+$ and $Au_2S(CH_2)_{15}CO_2CH_3^-$, are shown in Figure 6. Additionally, no new peaks are observed. Obviously, Au deposited on the CO_2CH_3 film behaves in a fashion similar to that for deposition on the CH_3 film; that is, Au atoms penetrate through the CO_2CH_3 film and form smooth buried layers under the film. At the same time, no chemical reactions occur.

(56) Since the presence of the oxidized headgroup will result in the loss of the strong S−Au chemisorption bonding, we speculate that the local vicinity will show enhanced susceptibility to Au penetration. The formation of columns or filaments of Au metal extending to vacuum interface then could act as a nucleation point for further deposited Au atoms, resulting in a local overlayer deposit of Au which could then increasingly block release of HSO_4^- fragments during SIMS analysis. While we presently do not have data to confirm this mechanism, we note that these results do indicate that one can expect the behavior of alkanethiolate SAMs under Au deposition to vary according to the chemical purity.

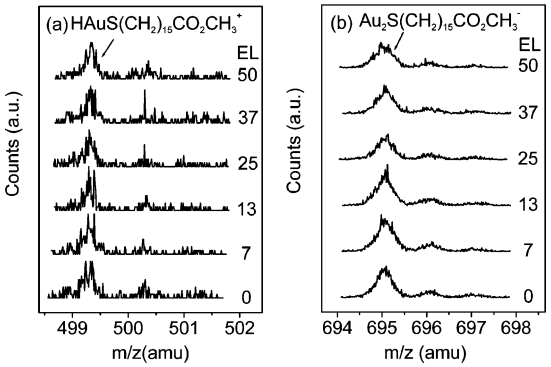

Figure 6. ToF−SIMS spectra obtained from a CO_2CH_3 film with increasing amounts of Au deposition: (a) $HAuS(CH_2)_{15}CO_2CH_3^+$; (b) $Au_2S(CH_2)_{15}CO_2CH_3^-$.

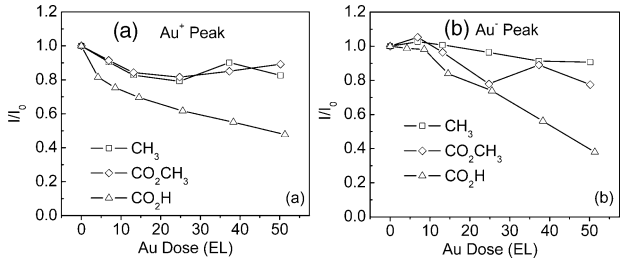

Figure 7. Relative intensities of Au^+ and Au^- peaks as a function of evaporated Au dose: (a) Au^+ peak; (b) Au^- peak. I_0 is the original intensity of Au^+ or Au^- peaks before Au deposition.

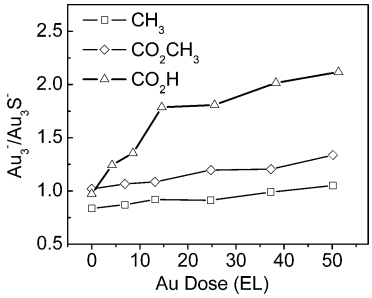

Figure 8. Ratio of Au_3^-/Au_3S^- as a function of evaporated Au dose.

Au on CO_2H SAM. For the CO_2H film, characteristic positive ion peaks and negative ion peaks considerably decrease in intensity with Au deposition when compared with the CH_3 and CO_2CH_3 systems. The trend for Au^+ and Au^- intensity for the CH_3, CO_2CH_3, and CO_2H films with Au deposition is shown in Figure 7. The ratio of Au_3^-/Au_3S^- considerably increases for the CO_2H film (Figure 8). Clearly, Au atoms do not form smooth layers under the film. Here, a reasonable explanation is that a fraction of Au atoms stay on top. Presumably, H-bonds between CO_2H groups prevent the Au atoms from formation of smooth buried layers. It is likely that the Au atoms on top of the film form clusters or islands instead of smooth layers at the vacuum interface, because, after deposition of 51 EL of Au, only 40% of the original intensity of those characteristic peaks remains (see Figure 9). Additionally, no new ion peaks were found during Au deposition, indicating no chemical reactions between CO_2H groups and Au atoms.

Previous work has shown that vapor-deposited Ag atoms accumulate on top of the $S(CH_2)_{15}CO_2H$ SAM and then slowly

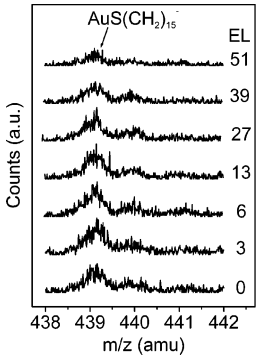

Figure 9. $AuS(CH_2)_{15}^-$ ToF−SIMS spectra obtained from a CO_2H film with increasing amounts of Au deposition.

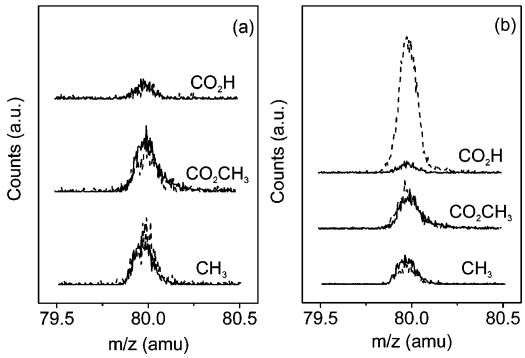

Figure 10. Comparison of SO_3^- peaks in the negative ion spectra of CH_3, CO_2CH_3, and CO_2H films before (solid line) and after (dash line) 2-h exposure in air: (a) freshly prepared samples; (b) samples after 13 EL of Au deposition.

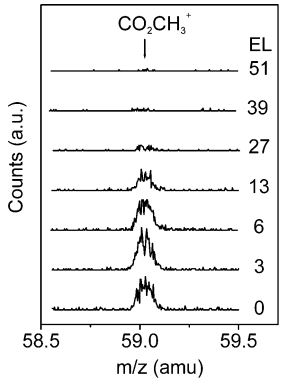

Figure 11. $CO_2CH_3^+$ ToF−SIMS spectra obtained from the 1.2 EL of K-modified CO_2CH_3 film with increasing amounts of Au deposition.

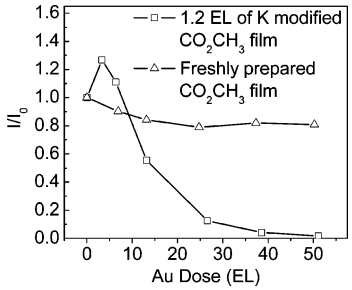

Figure 12. Relative intensities of $CO_2CH_3^+$ peaks as a function of evaporated Au dose. I_0 is the original intensity of $CO_2CH_3^+$ peak before Au deposition. The signal increase after 3.3 EL of Au deposition for K-modified CO_2CH_3 film is most probably due to an increase in sputtering yield due to the presence of Au.

penetrate through.[31] We believe that a fraction of the Au atoms penetrate through the CO_2H film, because Au is less active in interactions with terminal groups than Ag;[20] viz, the Au−CO_2H interaction should be weaker than the Ag−CO_2H interaction. It is impossible, however, on the basis of SIMS data alone, to determine which is the main channel, penetration, or cluster formation at the vacuum interface. The AFM and CPAFM results to be discussed later show the effects of metallic filaments penetrating through the film.

Exposure in Air. It is known that the weak SO_3^- and HSO_4^- peaks are found in the negative ion spectra. The SAMs are generally stable in air, at least for 2 h (Figure 10a), indicating that the films are impermeable to oxygen in air. After ~13 EL of Au deposition, however, different films show different oxidation resistance. From Figure 10b, one can conclude that the CH_3 and CO_2CH_3 SAMs are still impermeable to oxygen but that the CO_2H system is not. Our explanation is that for the CH_3 and CO_2CH_3 systems, Au atoms evenly penetrate through the film and form smooth underlayers. The compact structure of the organic thin films remains intact and the films are still impermeable to oxygen. For the CO_2H film, filaments or 3-d Au clusters form on the Au substrate as evidenced by our CPAFM data (see AFM section). Theoretically, the H-bond network reduces the possibility of penetration of Au atoms through the CO_2H film as compared to the CH_3 or CO_2CH_3 films. But at some special areas where the H-bond network is weak, such as defect areas or domain edges, Au atoms might easily pass through. After penetration of Au atoms, the H-bond network becomes weaker due to the changing substrate topography, resulting in more Au penetration in these areas. The compact structure of the CO_2H film would be partially diminished by formation of the filaments or 3-d Au clusters, thus allowing enhanced diffusion of oxygen molecules to the Au/S interface where oxidation of the S atoms could occur.[56]

Au on 1.2 EL K-Modified CO_2CH_3 SAM. To test the influence of chemically modified SAMs on Au penetration, 1.2 EL of K was deposited on a CO_2CH_3 sample before Au evaporation. Previous ToF−SIMS data[14,15] have shown that atomic K atoms can react with CO_2CH_3 groups and form CO_2K moieties and infrared spectroscopy data quantitatively confirm this (see Supporting Information). Both techniques show that 1.2 EL of K only reacts with 50−60% of CO_2CH_3 groups and there are still 40−50% CO_2CH_3 groups remaining. In the SIMS spectra, the CO_2CH_3 group related ion peaks, such as $OCH_3^{\pm}$, $CO_2CH_3^+$, and $Au_2S(CH_2)_{15}CO_2CH_3^-$, are still clearly observed. These peaks decrease very rapidly with Au deposition. The behavior of $CO_2CH_3^+$ with Au deposition is shown in Figure 11. The $CO_2CH_3^+$ peak intensity trend compared to the Au/CO_2CH_3 system is shown in Figure 12. It is very clear that the signal decrease rate for the K-modified sample is much faster. All CO_2CH_3-related peaks drop to a low intensity after 51 EL of Au deposition, strongly suggesting that most of the Au atoms stay on top of the K-modified CO_2CH_3 film instead of penetrating to the Au/S interface.

Au on 1.2 EL K-Modified CO_2H SAM. To test the behavior of a CO_2K surface, 1.2 EL of K was evaporated onto a CO_2H SAM. This dose is known to convert all of the CO_2H groups to CO_2K moieties from both ToF−SIMS[14,15] and infrared spectroscopy data (see Supporting Information). Au deposition onto this surface yields several intriguing intensity changes. As shown in Figure 13, the Au^+ signal itself has almost disappeared after

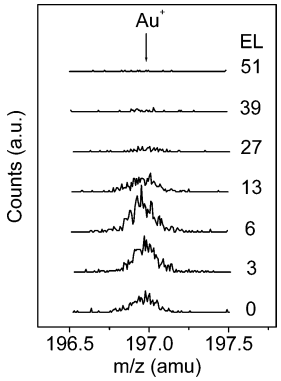

Figure 13. Au^+ ToF−SIMS spectra obtained from the K-modified CO_2H film with increasing amounts of Au deposition. The signal increase after 3 and 6 EL of Au deposition is most probably due to an increase in sputtering yield.

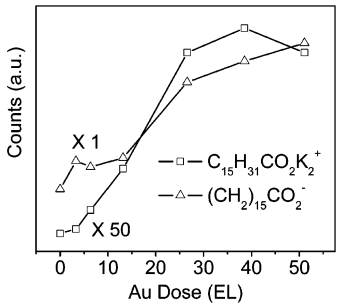

Figure 14. Intensities of $C_{15}H_{31}CO_2K_2^+$ and $(CH_2)_{15}CO_2^-$ peaks of the 1.2 EL of K-modified CO_2H film as a function of evaporated Au dose.

51 EL of Au deposition. This result suggests, somewhat counterintuitively, that the Au atoms are remaining on the surface of the organic film. Clean metallic Au exhibits a very weak Au^+ signal intensity due to resonance charge neutralization,[57,58] and the normally intense Au^+ emission arising from the Au−S interaction is effectively blocked by the metallic Au overlayer.

Additional intensity changes associated with the large molecular fragment $C_{15}H_{31}CO_2K_2^+$ and $(CH_2)_{15}CO_2^-$ as a function of Au deposition are shown in Figure 14. These signals steadily increase as the Au deposition occurs. This observation is consistent with the formation of 3-dimensional nanoclusters of Au atoms forming on top of the SAM layer. It is well-known that metal vapor deposition or metal nanoparticle deposition onto polymer surfaces significantly enhances the SIMS signal.[59−61]

The 1.2 EL K-modified CO_2CH_3 SAM exhibits similar behavior to the CO_2H SAM. The Au^+ signal decreases and the $C_{15}H_{31}CO_2K_2^+$ and $(CH_2)_{15}CO_2^-$ ions increase during Au deposition. Hence, we believe most of Au atoms remain at the vacuum interface.

AFM Results. Au Deposition on the CO_2H SAM. Contact mode images of a bare CO_2H SAM (Figure 15A) reveal the level of cleanliness and integrity of the surface as shown by the appearance of large underlying Au(111) terraces with well-defined step edges. The minor appearance of small clusters (∼1 nm in height) scattered across the surface is speculated to be due to clusters of H-bonded dimers between the $-CO_2H$ groups of SAM molecules and solute $HS(CH_2)_{15}CO_2H$ molecules. Extensive cleaning with dilute HCl solution minimizes the presence of these features, but in no case were we able to completely eliminate their appearance. Attempts to use other published cleaning techniques were found to be unsatisfactory and did not yield consistent results.[62] CPAFM images taken of the surface show a uniform and completely insulating film (data not shown).

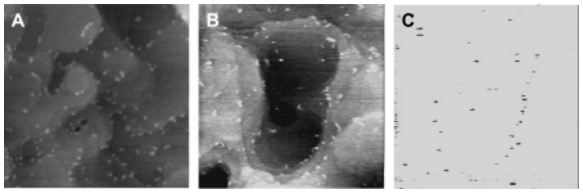

Figure 15. Images of a CO_2H SAM before and after vapor deposition of gold. All images are 1 μm × 1 μm in area. (A) Contact mode image of the bare SAM after HCl solution cleaning. The image clearly reveals the (111) terraces and step edges of the underlying gold. The small elevated (lighter shades) features are speculated to be H-bonded dimers of a SAM molecule and a $HS(CH_2)_{15}CO_2H$ molecule from the incubation solution. The corresponding CPAFM probe of this region shows a fully insulating behavior. (B) Contact mode image taken after deposition of gold to a coverage of 1.0 EL. The image still clearly reveals the structure of the underlying Au(111) substrate. The small elevated features appear to be the original intrinsic features in the bare SAM and possibly some gold clusters. (C) CPAFM current image recorded simultaneously with the topography image in (B) shows a number of electrical shorts in an otherwise fully insulating film. The shorts indicate the formation of Au filaments connected to the Au substrate. Comparison of topography and CP images shows that not all clusters are shorted.

In the initial stages of Au deposition up to ∼5 ELs, the surface topography revealed by contact AFM shows no detectable changes from the bare monolayer, as seen in Figure 15B. Importantly, no rough features or amorphous regions are observed on the Au(111) grains that might indicate Au cluster growth. This agrees with previous reports[4,5] that the Au atoms penetrate through the SAMs and diffuse across the Au/S interface to form a commensurate structure with the underlying Au, allowing an ordered SAM film to "float" above the Au substrate. Inspection of simultaneously recorded current images, however, shows small regions (points) of high conduction (Figure 15C). Since these features are not observed for the bare monolayer, the conduction pathways must arise from the Au deposition and we attribute them to nanofilaments of Au, which grow upward from the surface of the substrate. Filaments with lengths less than the thickness of the SAM (∼2 nm) are difficult to detect using contact mode AFM since the large radius of curvature of the tip and the shape of the contact interface would normally prevent a response of the cantilever to such a small buried feature.[63] By using the tip as a conducting probe, however, it is possible to detect the presence of such buried filaments since they can form conduction pathways to the Au substrate via tunneling from the tip without direct contact. The amount of current through these conduction pathways was found to vary greatly from hundreds of pA up to a complete short, at −10 nA,[64] and is attributed to different lengths and shapes of Au filaments formed on the surface of the Au(111). The highest current (total shorts) features are attributed to filaments longer than the monolayer thickness (∼2.0 nm[65]).

(57) Yu, M. L. *Phys. Rev. Lett.* **1978**, *40*, 574−577.
(58) Yu, M. L. *Phys. Rev. Lett.* **1981**, *47*, 1325−1328.
(59) Delcorte, A.; Medard, N.; Bertrand, P. *Anal. Chem.* **2002**, *74*, 4955−4968.
(60) Delcorte, A.; Bour, J.; Aubriet, F.; Muller, J. F.; Bertrand, P. *Anal. Chem.* **2003**, *75*, 6875−6885.
(61) Marcus, A.; Winograd, N. *Anal. Chem.* **2006**, *78*, 141−148.
(62) Wang, H.; Chen, S.; Li, L.; Jiang, S. *Langmuir* **2005**, *21*, 2633−2636.
(63) Carpick, R.; Salmeron, M. *Chem. Rev.* **1997**, *97*, 1163−1194.

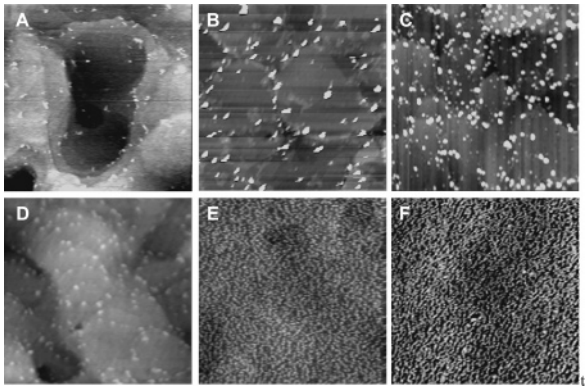

Figure 16. Contact mode AFM images (1 μm × 1 μm) of a CO_2H SAM surface after vapor deposition of Au and K followed by Au: (A) after deposition of 1.0 EL of Au atoms on a bare SAM surface (the same image as in Figure 15B shown for comparison purposes); (B) the same surface as in (A) but at a total coverage of 10 ELs; (C) the same surface as in (A) but a total coverage of 20 ELs; (D) after deposition of 1.0 EL of K atoms on a bare SAM surface; (E) the same surface as in (D) but with a total coverage of 10 ELs of Au; (F) the same surface as in (D) but with a total coverage of 20 ELs of Au. The accompanying rms roughness of the surfaces in (E) and (F) increases from 0.9 to 1.3 nm, consistent with the increased cluster surface density.

Indirect evidence from SIMS spectra also supports the formation of filaments in the initial stage. For example, the slight increase in the $AuS(CH_2)_{15}^-$ peak after 3 and 6 EL of Au deposition (Figure 9) is consistent with the appearance of Au formations located at or near the vacuum interface.

As the Au coverage increases, filament growth through the monolayer becomes more apparent in both topography and current images. For example, in Figure 16, comparison of images A−C at 1.0, 10, and 20 EL of Au atoms show the presence of increasing numbers of large clusters of Au growing on the surface. The large clusters vary in height up to ∼10 nm. Simultaneous CPAFM images recorded for the two highest coverages (data not shown) reveal electrical shorts at all of the clusters, indicating formation of mushroomlike structures. We note that high-quality topographical images are difficult to obtain for these coverages since the high number of electrical shorts causes increasing wear on the AFM tips.

Au Deposition on K-Coated CO_2H Monolayer. Inspection of the topography of the CO_2H SAM surface after deposition of 1.0 EL of K shows only a uniform surface with no significant new features (compare parts A and D of Figure 16). Independent IR data (see Supporting Information) shows that at this K coverage all the CO_2H terminal groups have reacted with the K atoms to form carboxylate species, thus dictating that the K coverage must be uniform. After deposition of Au at coverages from 1 to 5 ELs on the K-dosed surface, the initial contact mode AFM images show large streaks in the images indicative of mobile particles on the top of the monolayer surface (data shown in the Supporting Information). At higher Au coverages, however, the streaking vanishes, the same images appear with continued scanning, and the Au morphology is observed as a continuous "wormlike" structure over the entire surface (Figure 16E,F), dramatically different from the isolated filaments observed in the $-CO_2H$ surface with no K (Figure 15). It is likely that this "wormlike" structure consists of the Au overlayer as the higher elevated parts of the structure with the SAM surface in the pits. With increasing doses the Au both covers increasing areas of the surface and is elevated increasingly higher above the pits (compare parts E and F of Figure 16). This is consistent with an increase in rms surface roughness from 0.9 to 1.3 nm for the increasing coverages. Comparison of the images of the 10 and 20 Au equivalent monolayer images for the K-dosed and the bare SAM surfaces (compare Figure 16E,F with Figure 16B,C) shows that the K dosing causes a dramatic increase in the affinity for the Au atoms to form an overlayer as opposed to penetration through the SAM. Measurements of the current differences between the peaks and valleys of the "wormlike" structure via CPAFM images were unsuccessful due to the large, destructive currents involved, but it is quite clear in the case of the K-dosed samples that the entire gold overlayer is in electrical contact with the substrate.

Overall Summary of the AFM Data. There are two main findings from the AFM data. First, the deposition of Au on the bare CO_2H SAM results primarily in penetration through the SAM, higher gold coverages lead to increasing formation of isolated gold features at or near the surface, and these features are generally correlated with electrical conducting metal filaments connected to the underlying Au substrate. Second, in the case of a SAM surface dosed with 1 EL of K, the K atoms are uniformly distributed across the surface and further deposition of Au onto this surface results in dominant formation of an electrically interconnected gold overlayer, which has conducting pathways to the substrate. Thus, the presence of a deposited K layer serves to block penetration of the Au atoms to the substrate to a major extent but does not block the formation of electrical shorts to the substrate. These results are consistent with the SIMS data presented earlier.

Structural Correlations Underlying Au Partitioning between Overlayer Growth and SAM Penetration. Previously, a penetration mechanism of evaporated metals on SAMs has been proposed.[9] With this model, if the interaction between metal atoms and surface organic functional groups were weak, metal atoms could pass through thermally created temporary vacancies between film molecules. For the CH_3 and CO_2CH_3 systems, only van der Waals interactions exist between film molecules, and Au atoms penetrate through the films evenly to form smooth layers under the film as illustrated in Figure 17a.

Average H-bond energies, typically ∼10−20 kJ/mol, are significantly larger than thermal energy at room temperature. Theoretically, a full network of H-bonds between film molecules should block metal penetration, a result that is not observed. At low coverages (5 ELs), most Au atoms penetrate through the CO_2H film, with formation of a few Au filaments. With an increasing Au dose, 3D clusters are gradually formed at the vacuum interface. CPAFM shows that all such clusters are shorted to the Au substrate, and the shape of these clusters is like a "mushroom", as illustrated in Figure 17b. This observation can be attributed to the structure of the CO_2H film.[12,13,66−68]

(64) −10 nA was the high current limit set for the current amplifier for these experiments. The voltage was limited to −10 mV since higher voltages were found to create currents high enough to damage the tip; this high current can lead to complete demetallization of the contact area of the tip. This is unfortunate since higher voltages could be used to probe deeper into the monolayers enabling better imaging of filament growth beneath the alkanethiol surface.

(65) Shi, J.; Hong, B.; Parikh, A. N.; Collins, R. W.; Allara, D. L. *Chem. Phys. Lett.* **1995**, *246*, 90−94.

(66) Dannenberger, O.; Weiss, K.; Himmel, H. J.; Jager, B.; Buck, M.; Woll, C. *Thin Solid Films* **1997**, *307*, 183−191.

(67) Arnold, R.; Azzam, W.; Terfort, A.; Woll, C. *Langmuir* **2002**, *18*, 3980−3992.

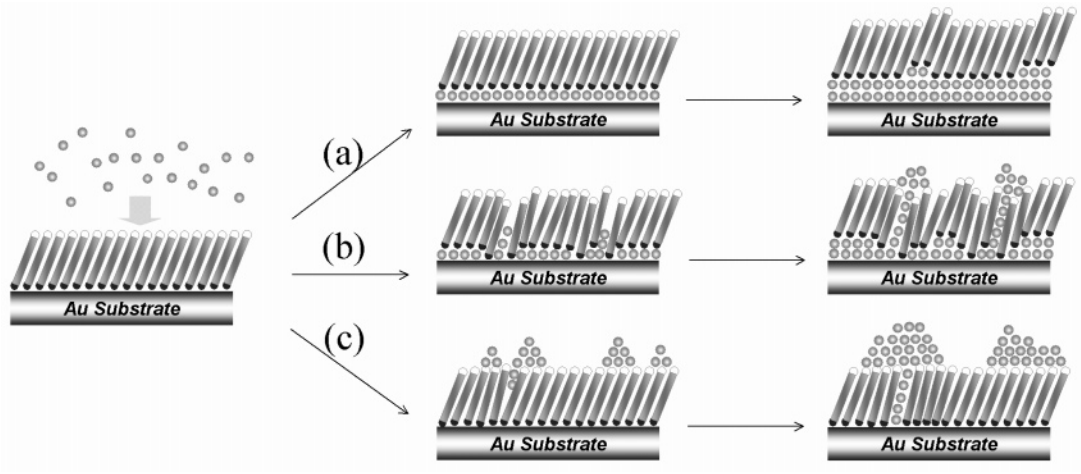

Figure 17. Schematic illustration of Au behaviors on different SAMs: (a) continuous, uniform penetration leading to smooth buried underlayers, as seen for Au on the CH_3 and CO_2CH_3 SAMs; (b) at low coverages, penetration of Au to form a buried underlayer with some formation of buried islands and initial growth of some filaments and, at higher coverages, penetration of Au to form conducting filaments with connected overlayer clusters, as seen for Au on the CO_2H SAM; (c) at low coverages, nucleation of overlayer clusters with initial scattered penetration into the SAM and, at higher coverages, penetration leading to formation of scattered conducting filaments connected to overlayer clusters in mushroomlike overlayer deposits and contiguous overlayer islands, as seen for Au on the K-modified CO_2CH_3 and CO_2H films.

The stereochemistry of the O atoms and H atoms make the strength of such H-bonds relatively weak, and it has been estimated that 20% or more CO_2H groups are free of H-bonding.[12,13] Additionally, at the defect areas and domain edges, H-bonds cannot form an effective network. Therefore, Au atoms can still considerably penetrate through the CO_2H film.

In contrast to the CO_2H SAM, the CO_2K functionality is effective in blocking metal penetration. Two reasons to consider are an enhanced nucleation of Au atoms at the K^+ sites because of more favorable energetic interactions than with the CO_2H surface or a reduction in the dynamic vacancy mechanism rate due to increased intermolecular binding relative to the CO_2H case. Given the relatively low polarizibility of the positively charged K^+ species, however, it does not seem likely that there would be a significant enhancement of Au atom surface binding with formation of high nucleation site densities at the ionic vs the CO_2H surface. On the other hand, given that the strength of ionic interactions (generally several hundred kJ/mol[69,70]) is orders of magnitude higher than thermal energy at room temperature and considering that the K^+ ions and CO_2^- ions are constrained by the underlying SAM structure to form a uniformly structured layer, one can expect the activation barrier for formation of transient vacancies in the SAM to be substantially larger than for the cases of only van der Waals or H-bonding interactions. Accordingly, the majority of Au atoms would remain on top of the CO_2K layer where they can diffuse to form clusters. We note that our CPAFM data, however, show that the top Au clusters are shorted to the Au substrate, so there must be some degree of penetration to the substrate with formation of filaments to serve as conduction paths. One possible mechanism contributing to penetration is that the interface between K^+ ions and CO_2^- ions is disrupted at domain edges or step cases, thereby lowering the barrier to Au penetration in this region.

Conclusion

The behavior of vapor deposited Au on CH_3, CO_2CH_3, CO_2H, K-modified CO_2CH_3, and K-modified CO_2H SAMs has been investigated by ToF−SIMS and AFM. Au atoms penetrate through CH_3 and CO_2CH_3 films evenly and form smooth buried layers under the organic thin films. The compact structure of the films remains. Electrically conducting filaments, some with large clusters growing out at the vacuum interface (mushroomlike), are found in the Au/CO_2H system. Most Au atoms stay on top of the K-modified CO_2CH_3 and CO_2H films and form islands on the organic thin films, indicating that the CO_2K layer is an effective buffer layer to block metal penetration.

Our results show that it is possible to exercise some control over Au penetration through the alkanethiol SAMs by adjusting the interactions between film molecules. For weak van der Waals forces the films are permeable to Au atoms, such as the CH_3 and CO_2CH_3 films. The H-bonding web in CO_2H film is not strong enough to block penetration. In contrast, ionic interactions are found to be strong enough to prevent significant penetration of Au atoms. We believe these types of correlations will be beneficial for the design and fabrication of metal/organic thin film/metal sandwich structures, which are widely used in measurements of electronic properties of functional organic molecules. Thus, the ability to control the morphologies and placement of deposited metal atoms in organic films includes not only the ability to vary the type of metal atom−organic chemical interactions, e.g., use of $-OCH_3$ groups to complex Al atoms to reduce penetration,[17,20] but the ability to tailor the intermolecular interactions at specific locations along the chain by tuning of van der Waals, H-bonding, and ionic interactions that can lead to control of competing diffusion and nucleation channels in the case of lower reactivity and inert metals.

Finally, our results show that combining ToF−SIMS and AFM is an efficient strategy to characterize metal/SAM/metal sandwich structures. Chemical information can be extracted from SIMS spectra and topography and conductivity information from

(68) Willey, T. M.; Vance, A. L.; van Buuren, T.; Bostedt, C.; Nelson, A. J.; Terminello, L. J.; Fadley, C. S. *Langmuir* **2004**, *20*, 2746−2752.
(69) Gasgnier, M.; Petit, A. *J. Mater. Sci.* **1994**, *29*, 6479−6484.
(70) Lide, E. R.; Ed. *Handbook of Chemistry and Physics*; CRC Press: Boca Raton, FL, 1995; Vol. 1976, pp 12−19.

AFM data. This combination provides a rather complete picture of the resulting film properties.

Acknowledgment. We gratefully acknowledge financial support from the National Science Foundation (NSF), in particular the Center for Nanoscale Science (MRSEC, DMR No. 0213623, T.A.D.).

Supporting Information Available: Infrared reflection spectroscopy titration for K addition to the CO_2H and CO_2CH_3 SAMs and initial contact and current mode AFM images of Au deposited on the K-treated CO_2H SAM. This material is available free of charge via the Internet at http://pubs.acs.org.

JA060084X